Desalination and Water Treatment
www.deswater.com

doi: 10.5004/dwt.2022.29020

280 (2022) 76–88
December

Sintering effect on cationic and anionic dyes adsorption efficiency using natural red clay: limitations and future scope of the study

H. Jazi*, A. Ezzahi, A. Karim, D. Machtani Idrissi, M. Bouhria, S. Alami Younssi

Laboratory of Materials, Membranes and Environment, Faculty of Sciences and Technologies Mohammedia, University Hassan II, Casablanca, Morocco, emails: hind.jazi-etu@etu.univh2c.ma/jazi.hind.18@gmail.com (H. Jazi), amine.ezzahi@fstm.ac.ma (A. Ezzahi), karimabdelaali@gmail.com (A. Karim), elmachtanidoha@gmail.com (D. Machtani Idrissi), mohamed.bouhria@fstm.ac.ma (M. Bouhria), saad.alamiyounssi@fstm.ac.ma (S. Alami Younssi)

Received 21 January 2022; Accepted 7 October 2022

ABSTRACT

This work aims to evaluate the sintering effect on adsorption efficiency to remove cationic and anionic dyes from aqueous solutions using Moroccan red clay. The adsorption experiments were carried out and the effect of adsorbent amount, medium pH, contact time, concentration and temperature on the removal process was investigated. Herein, to understand the adsorption phenomenon, raw clay was characterized in terms of chemical composition (X-ray fluorescence), mineralogical composition (X-ray diffraction), thermal analysis (TGA), spectroscopic analysis (Fourier transform infrared spectroscopy) and Brunauer–Emmett–Teller (BET) specific area. This study suggests that the raw red clay exhibits strong adsorption when compared with sintered red clay for cationic dye rather than anionic (99.30% for methylene blue (MB) and 0.01% for methyl orange (MO)). The adsorption equilibrium data obtained at 25°C were simulated by Langmuir and Freundlich isotherm models. The experimental results indicate that the adsorption efficiency is stable at different pH. The maximum adsorption capacity for removal was 25 and 5 mg/g for raw red clay (RRC) and sintered red clay (SRC) respectively. The adsorption isotherm of MB on RRC and SRC was also investigated. Experimental data fitted by using Langmuir equation gives an R^2 of 0.969 and 0.978, respectively, for RRC and SRC. For both adsorbents, the pseudo-second-order kinetics is the most suitable model. As a result, the thermodynamic study indicates that the adsorption process is spontaneous and exothermic on RRC but for SRC the process is endothermic and not spontaneous. The obtained results show that both adsorbents are highly effective for MB cationic dye removal and not for MO anionic dye removal.

Keywords: Adsorption; Natural red clay; Sintering; Methylene blue; Methyl orange

1. Introduction

Significant growth in industrial and urban activities produce polluted wastewater that is largely contaminated with organic compounds. Synthetic dyes are used in various industries such as textiles, cosmetics, paper and food [1], and are a major cause of environmental problems due to their high risk factor, especially for water resources. This type of pollution creates an imbalance in the environment through its visual impact, especially the deterioration of natural aquatic life. In addition, the infiltration of these compounds into soil can affect the quality of groundwater [2,3]. For these reasons, it is necessary to implement a proper treatment process to overcome these environmental problems.

* Corresponding author.

Presented at the Second International Symposium on Nanomaterials and Membrane Science for Water, Energy and Environment (SNMS-2021), June 1–2, 2022, Tangier, Morocco

In order to treat wastewater, many treatment processes such as membrane filtration [3–5], physicochemical treatments [6] and coagulation–flocculation [7] have been widely used to remove dyes and pollutants from effluents. However, these different techniques are reported to be limited by the performance/cost ratio [1]. The adsorption process has received increasing attention as it is considered to be the simplest and most efficient technique used in various industries, especially in dye removal [8–10]. Furthermore, this environmental-friendly process does not require much energy or complex facilities to be implemented [11].

Over the past decade, many published studies have focused on developing new alternatives to well-known adsorbents such as activated carbon and its derivatives [12–14]. Hence, due to their high manufacturing cost, environmental-friendly methods have been proposed. More recently, Mahmoodi et al. produced inexpensive activated carbons from various vegetable sources such as kiwi fruit peel, cucumber peel and potato peel to remove dyes in single- and multi-component systems [4]. From the same point of view, adsorption based on organic wastes such as orange peel, wood, palm trees and nuts has received extensive attention [15–19], while cellulosic materials of agricultural origin have also been used for methylene blue elimination [20].

On the other hand, natural inorganic materials have proved their high ability to remove organic dyes. Clay, phosphogypsum, pozzolan and perlite constitute a research board for the development of natural adsorbents because of their structures and abundance [21–25]. Jawad et al. [26] achieved a maximum adsorption capacity of 240.4 mg/g at 303 K for methylene blue on red kaolin clay while Avila et al. [27] used treated bentonite to eliminate methyl orange and attended an adsorption capacity of 125 mg/g. Muscovite clay was the subject of many works as adsorbent. Amrhar et al. [28] has studied the adsorption of methylene blue from aqueous solution using Monte Carlo simulation. Muscovite/phillipsitic zeolite composite are used for the elimination of heavy metals from water [29]. Barakat et al. [30] studied the efficiency of muscovite-supported iron oxide as an adsorbent and heterogeneous catalyst for the absorption of azo dyes. To the best of our knowledge, only few research works have been reported on the effect of sintering on adsorption capacity using natural clay as adsorbent [31]. Red clay used in this study is characterized by its abundance and null shrinkage property, which makes it suitable for use in various fields of applications. For example, it has a large application in different Moroccan industries such as bricks [32], tiles, pottery as well as in the fabrication of membranes. The effect of sintering on the properties of clay as fascinated products is very important to predict the level of contamination after use in specific mediums as in the case of pottery. In addition, the adsorption study after sintering can also help to identify the fouling level on membranes made from red clay.

The main objective of this work is to valorize natural local material in the environmental fields specifically for dye removal. The natural red clay is used to evaluate its capacity for anionic and cationic dye removal. Furthermore, the effect of sintering at 950°C on adsorption capacity was examined. The study is focused on the elimination of MB and MO dyes from aqueous solutions using raw (RRC) and sintered clay (SRC). The effect of adsorption parameters such as pH, dose, time, dye concentration and temperature was studied. The isotherms and kinetic models were established.

2. Experimental setup

2.1. Raw materials

The clay sample used in this study was collected from Ben Ahmed – Settat region and it had a dark brown color [32]. Two commercial cationic and anionic dyes, respectively, methylene blue (MB) and methyl orange (MO) were supplied by Loba Chemie (India). Distilled water was obtained using a laboratory distiller. Sodium hydroxide (NaOH) and hydrochloric acid (HCl) used for pH adjustment were provided by Sigma-Aldrich (Germany). Also, sodium nitrate ($NaNO_3$) used for the determination of pH zero-charge point (pH_{PZC}) was also supplied by Sigma-Aldrich. All chemical products were used without any treatment.

2.2. Preparation of adsorbents

Clay sample was first crushed, ground and sieved through a 160 μm sieve to obtain a fine portion, which is denoted as raw red clay (RRC). Afterwards, a part of the RRC powder was sintered at 950°C using the thermal treatment sintering program presented in Fig. 1; then this process was followed by sieving at 160 μm to remove the agglomerated grains. The resulting sample is called sintered red clay (SRC):

2.3. Characterization techniques

Red clay sample was identified by different characterization techniques. Chemical composition was determined by X-ray fluorescence (XRF) (Axios-Malvern Panalytical, UK). The mineralogical characterization was performed using X'Pert PRO X-ray diffractometer (Malvern Panalytical, UK) employing CuKα radiation (1.5418 Å) at a goniometer rate of $2\theta = 4°$/min. Fourier transform infrared spectroscopy (FTIR) was carried out using a Shimadzu (Shimadzu, Kyoto, Japan) (Affinity-1S) spectrometer equipped with a Golden Gate (the single reflection) attenuated total reflectance attachment in the wavelength range of 400 to 4,000 cm^{-1}. The BET surface area is measured with an apparatus (Quantachrome Instrument TouchWin™, St 1 on NOVA touch 4LX [s/n: 1050021052], USA). The morphological structure was studied by scanning electron microscopy (SEM) using Quanta 200 (FEI Company, The Netherland).

Thermal analysis and differential scanning calorimetry (DSC) of used samples were conducted using a DSC/TGA simultaneous analyzer (SDT Q600, TA Instruments, DE, USA) with a heating rate of 5°C/min. The concentration of MB and MO dyes was measured by UV-Vis spectrophotometry (JASCO V-730 spectrophotometer, Tokyo, Japan) at a maximum wavelength of 664 and 582 nm, respectively.

2.4. Zero charge point

The pH_{PZC} is a very important factor in the adsorption phenomena to prospect the surface charge density of the

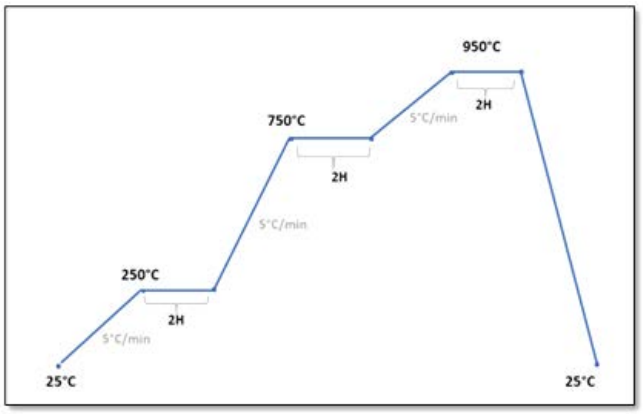

Fig. 1. Sintered red clay thermal program.

materials. To determine the pH_{PZC}, pH tests were performed by a simple and rapid method [28]. The method consists mainly of preparing a series of 10 samples of 50 mL volume of 0.1 M $NaNO_3$ solution and adjusting their pH from 2 to 11 by adding a solution of 0.1 M NaOH or 0.1 M HCl. It should be noted that the mass of both adsorbents (RRC and SRC) was fixed in 300 mg for each matrix. The prepared suspensions were kept under constant and soft agitation (250 rpm) at room temperature for 24 h to determine the final pH values. The zero-charge point (pH_{PZC}) was determined from the intersection of the pH variation curve $\Delta pH = pH_f - pH_i$ and initial pH of the solution.

2.5. Adsorption experiments

The method used on RRC and SRC for dye removal was based on static batch adsorption. First, a sequence of 50 mL beakers was prepared with different adsorbent amounts (50, 100, 200, 300, 400, 500, 800 and 1,000 mg) for discoloration of MB and MO solutions during 90 min, then, the resulting suspensions were separated by centrifugation and syringe filters. Finally, the supernatants were measured by a UV-Vis spectrophotometer. All experiments were carried out with an electrically thermostatic stirrer at 250 rpm.

In this study, several parameters were studied to identify the optimal values of pH, contact time, concentration and temperature for both samples. The pH values were adjusted to 2, 4, 6, 8 and 10 using NaOH 0.1 M and HCl 0.1 M solutions. Adsorption time was determined by measuring the rejection rate in the range of 5, 10, 15, 30, 45, 60 and 90 min. The effect of concentration on rejection was studied by varying the concentration of the solution from 10, 20, 30, 40, 50, 60 to 70 mg/L. To evaluate the effect of temperature on dye adsorption and to determine the thermodynamic parameters, different temperature values of 20°C, 30°C, 40°C, 50°C and 60°C were selected. The adsorption rate (R) was calculated by using the following equation:

$$R(\%) = \frac{C_i - C_f}{C_i} \times 100 \quad (1)$$

where C_i and C_f (mg/L) are the initial and final concentrations, respectively. The adsorption capacity q_e (mg/g) of RRC and SRC was calculated by using Eq. (2):

$$q_e = \frac{V}{M}\left(C_i - C_e\right) \quad (2)$$

where V is the solution volume (L), M is the adsorbent mass (g), C_i represents initial concentration and C_e indicates equilibrium concentration (mg/L).

3. Results and discussion

3.1. Clay characterization

3.1.1. Chemical composition

The chemical analyses of red clay were carried out using X-ray fluorescence spectrometers. The results are grouped in Table 1:

X-ray fluorescence analysis shows that the natural Moroccan red clay is characterized by the presence of 59.32% silica (SiO_2), 11.44% of alumina (Al_2O_3), 4.29% of iron oxide (Fe_2O_3) and 2.1% of calcite (CaO). Therefore, the highest percentage in terms of silicates is due to the presence of clay minerals and free silicates [33].

3.1.2. Mineralogical composition

The X-ray diffraction (XRD) diffractogram allows the identification of different mineral phases that constitute the raw and sintered clay as shown in Fig. 2. Examination of the XRD patterns shows the presence of quartz, calcite, muscovite, dolomite and hematite. It can be seen from the RRC that quartz minerals present the highest proportion. These results are in agreement with XRF analysis. The SRC pattern describes the conservation of dominant phases such as quartz and muscovite. However, the calcite and dolomite phases disappeared.

The XRD analysis shows that the thermal treatment transforms the calcite and dolomite structures into unstable structures and decomposes to CaO and MgO generating CO_2. This is confirmed by the disappearance of the dolomite and calcite peaks on the SRC spectrum [34,35].

3.1.3. Spectroscopic analysis (FTIR)

Fig. 3 shows the FTIR spectrums of RRC and SRC samples in the wavelength range of 400–4,000 cm^{-1}. The RRC spectrum shows the presence of two bands at 3,624 and 3,694 cm^{-1}, which are dedicated to the stretching of free hydroxyl groups (–OH). The thermal treatment abolished the bands on the SRC spectrum. Thus, the presence of a hydrogen bond between the adsorbed water and the surface of the clay is represented by a broad band appearing near 3,500 cm^{-1} [36].

The band with low intensity at 1,640 cm^{-1} is attributed to the deformation vibrations of the H_2O molecules adsorbed between layers [26]. Carbonates (C–O) are characterized by the presence of a slight peak at 1,429 cm^{-1}. During the heat treatment at 950°C, the band at 1,429 cm^{-1} might be shifted to 1,417 cm^{-1} and an intense and clear band shown at 3,644 cm^{-1} is due to the presence of $Ca(OH)_2$ [37]. The tetrahedral layer is indicated by an intense band at 996 cm^{-1} that corresponds to the valence vibration of

Table 1
X-ray fluorescence analysis of used raw clay

Element	Chemical composition (wt.%)
CuO	0.01
ZnO	0.02
P_2O_5	0.12
K_2O	0.18
SO_3	0.75
Na_2O	0.80
MgO	1.57
CaO	2.10
Al_2O_3	11.44
FeO_3	4.29
SiO_2	59.32

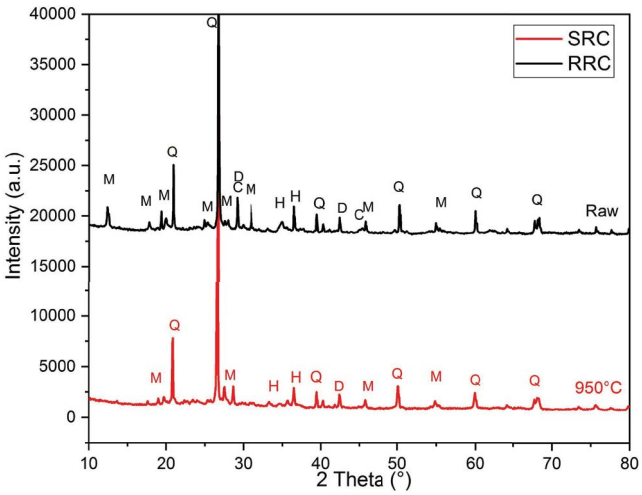

Fig. 2. X-ray diffraction patterns of raw red clay and sintered red clay samples.

Si–O. A doublet of low intensity at 780–798 cm^{-1} is due to inter-tetrahedral Si–O–Si bridging bonds in quartz [38].

3.1.4. Specific area (BET)

Specific area is an important parameter to estimate the capacity of material in terms of adsorption amount. The more the BET surface is higher, the more adsorption capacity is significant. In this study, the BET surface measurement was determined in the same conditions of preparation.

First, the samples were dried in the oven at 105°C for 24 h before analysis. Surface area, total pore volume and pore size distribution of RRC and SRC samples were determined from adsorption/desorption isotherms and realized in an adsorption apparatus (Quantachrome TouchWin™, St 1 on NOVA touch 4LX [s/n: 1050021052], USA) under ambient temperature of 33.89°C using liquid nitrogen (N_2) at a bath temperature of 77.35 K. The results were exported from the isotherm curve of adsorbed amount of N_2 as function of relative pressure. The BET specific area is expressed by m^2/g. The result of BET surface for RRC and SRC is,

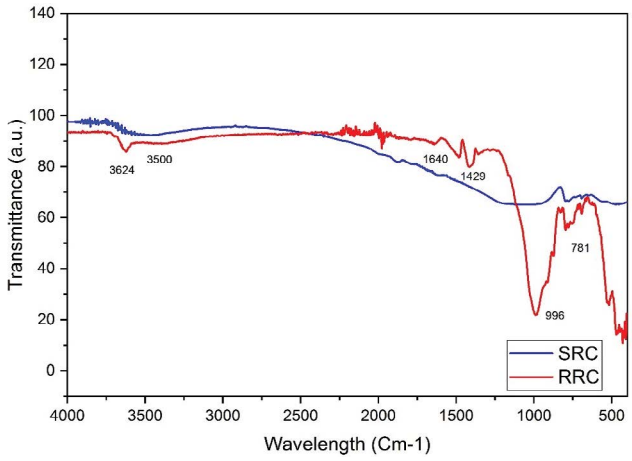

Fig. 3. Infrared spectrum of raw red clay.

respectively, equal to 12.605 and 4.475 m^2/g. The pore structure and pore size distribution characteristics were identified using *t*-plot and Barrett, Joyner and Halenda method (BJH) for the mesopores of samples. From the analysis, the pore volume and the average pore size distribution were 0.0371 cm^3/g and 3.362 nm for RRC and 0.0086 cm^3/g and 3.363 nm for SRC, respectively.

3.1.5. Scanning electron microscopy

Scanning electron microscopy was performed to observe the red clay particle texture and to characterize its mineralogical assemblages. SEM images illustrated in Fig. 4 were obtained with different magnifications. The clay particles are presented in the form of clusters of fine aggregates and platelets in the form of sticks with an automorphic form, which reveals the presence of quartz in the sample.

3.1.6. Thermal analysis (TGA)

Thermal analysis data of red clay samples present different weight losses, which could be explained by different phenomena. From Fig. 5, it was observed that the global weight loss was around 9.5 wt.% of the initial weight measured in the temperature range of 0–1,000°C.

The first mass loss observed before 200°C (about 1.7 wt.%) is dedicated to the elimination of sample moisture. The second loss from 200°C to 450°C is dedicated to the combustion of organic matter. The highest mass loss of 6% observed from 450°C to 700°C is composed of two segments; the first is due to hygroscopic water elimination by dehydroxylation of the structural (OH) and the second one that begins from 600°C is due to the decomposition of carbonates [39].

3.2. Adsorption experiments

The investigated clays, RRC and SRC, are used for MB and MO dye removal to evaluate their capacity against positive and negative charged dyes. The effect of sintering at 950°C on adsorption performance is also evaluated to predict the impact of thermal treatment on clay properties in other applications such as ceramic manufacturing [4,32,40,41].

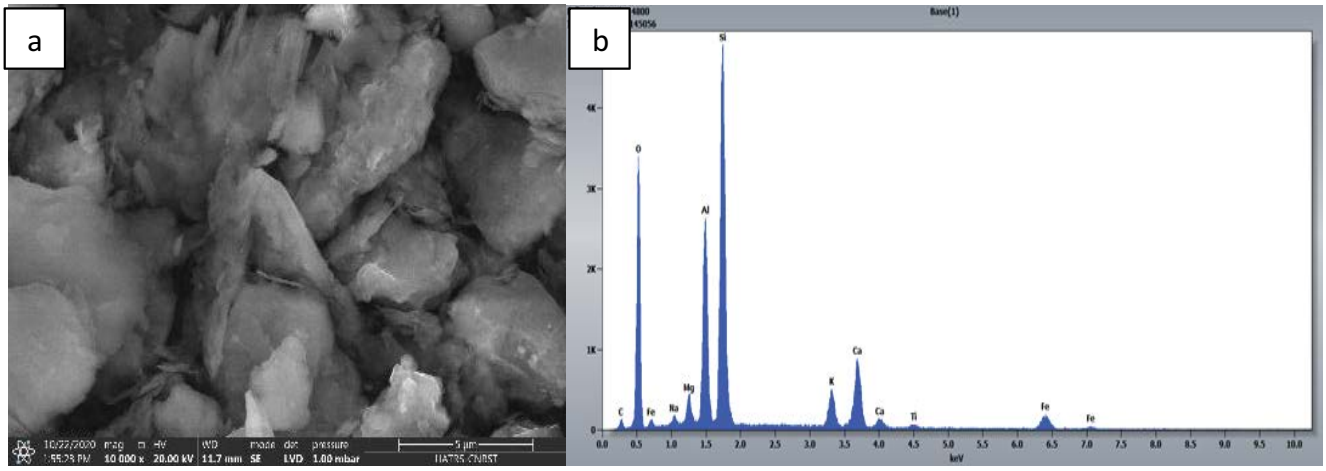

Fig. 4. Scanning electron microscopy pictures of raw red clay (a) and energy-dispersive X-ray spectroscopy analysis (b).

In addition, kinetics, thermodynamics and isotherm studies help to understand the behavior of RRC and SRC.

3.2.1. Effect of adsorbent dose

In order to optimize in terms of adsorbent mass, different amounts were applied for dye removal. In this case, RRC and SRC were evaluated for MB and MO dyes using the same fraction at different doses.

Fig. 6 shows the evolution of adsorption rate vs. adsorbent dosage. RRC and SRC present similar adsorption profiles for the adsorption of MB 50 ppm during 90 min. According to the figure, RRC and SRC achieve maximum adsorption rate using 100 and 200 mg, respectively. From the result, it could be noted that sintering at 950°C reduces the adsorption capacity of red clay by about 15%.

The same experimental protocol was used for MO 50 and 10 ppm. Appendix A (supplementary data) illustrates the evolution of MO removal as a function of RRC and SRC amounts. It can be concluded that SRC presents null affinity for MO, while RRC shows a maximum removal rate of 10% for both concentrations of MO. From these results, it can be concluded that red clay presents low affinity for MO negative dye. Moreover, the sintering at 950°C makes SRC free from positive sites.

As a result, 100 and 200 mg were considered as optimal doses for RRC and SRC clays, respectively, to determine other adsorption parameters for MB dye removal. On the other hand, even at 1,000 mg the adsorption of MO did not lead to any significant results. For this reason, other effects were not pursued.

3.2.2. Adsorption kinetics

The adsorption process was studied at initial concentration of 50 ppm, batch temperature of 25°C, optimum pH of 5.8 and time intervals of 5–90 min using 200 and 400 mg for RRC and SRC, respectively, at constant stirring speed of 250 rpm. Samples were collected and centrifuged for 5 min at 2,500 rpm before being characterized. Fig. 7 shows adsorption capacity as a function of contact time using RRC and SRC samples.

In the case of RRC, it demonstrates that during the first few minutes, adsorption was fast and dominant due to the availability of more vacant sites and reached a capacity value of about 22 mg/g. After 5 min, adsorption was proportionally slower up to 20 min (Fig. 7a) and this could be related to the slow diffusion of MB into the pores occupying the entire surface and structure sites of the clay. On other hand, the adsorption kinetic profile of SRC shows a slow adsorption rate during the first 30 min compared with RRC (Fig. 7b). The reaction takes place between the functional groups on the red clay surface or structure site and the positive charge of the MB aqueous solution through complexation or cation exchange with the negative charges of the red clay adsorbent surface. The same results were observed in the literature [24,42].

The modelization of experimental data using linear and non-linear kinetic models such as pseudo-first-order (PFO) and pseudo-second-order (PSO), respectively, was selected to study the MB adsorption using RRC and SRC samples.

Lagergren's PFO and Ho's PSO rate equations were applied to describe the kinetics of MB adsorption on RRC and SRC [22,24]. Kinetic models are expressed, respectively, in Eqs. (3) and (4). The amount of dye adsorbed per unit mass of clay as a function of time was calculated according to the first-order Lagergren rate equation, and defined as follows:

$$q_t = q_e\left(1 - e^{-K_1 t}\right) \tag{3}$$

where q_e, q_t, t and K_1 are, respectively, the equilibrium capacity (mg/g), adsorbed quantity (mg/g) at time t (min) and K_1 (g/mg min) is the rate constant of the adsorption process at equilibrium of PFO. This constant (K_1) can be determined experimentally by fitting the non-linear equation. Regarding the PSO model that is expressed by Eq. (4):

$$\frac{1}{q_t} = \frac{1}{K_2 q_e^2} + \frac{t}{q_e} \tag{4}$$

where K_2 is the rate constant of adsorption processes of the PSO model (g/mg min).

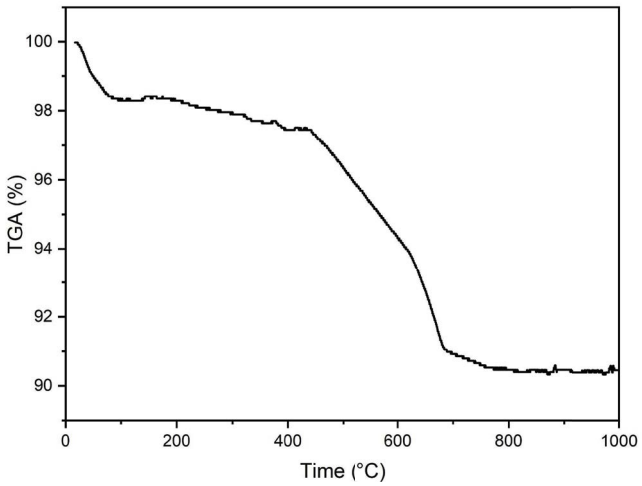

Fig. 5. Thermal analysis TGA of red clay.

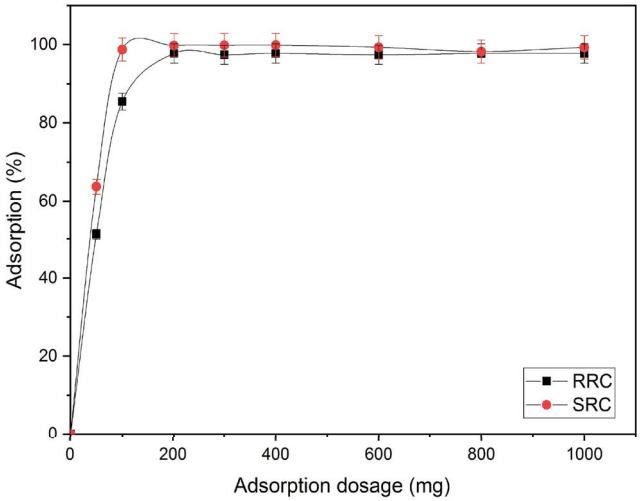

Fig. 6. Dose effect on adsorption capacity of sintered red clay and raw red clay for MB removal (50 ppm).

Fig. 8 shows the application of the kinetic models of PFO and PSO for the adsorption of MB on RRC and SRC. The values of the equilibrium adsorbed quantities q_e, model constants (K_1 and K_2) and the regression coefficients R^2 for both used samples are generated in Table 2.

The figure depicts that experimental data of both samples are more correlated by the PSO model (Fig. 8c and d) with correlation factor R^2 of 0.9998 and 0.9904, respectively, for RRC and SRC. Meanwhile, the values of R^2 generated from PFO fitting curves are 0.342 and 0.592, respectively, for RRC and SRC (Fig. 8a and b).

The obtained kinetic parameters of MB adsorption are presented in Table 2. The values of calculated amount of adsorbed dye at equilibrium ($q_{e,cal}$), PFO adsorption rate constant (K_1) and PSO adsorption rate constant (K_2) were generated from the slope or intercept of the straight line of the appropriate model. The applicability of each model was checked by the fitness of the straight lines (R^2 values) with the linear forms of the models.

Table 2
Constants of the Lagergren pseudo-first-order velocity equation and the Ho and McKay's pseudo-second-order equation

First-order	K_1 (min^{-1})	q_e (mg/g)	R^2
RRC	0.0451	0.061	0.342
SRC	0.0026	1.131	0.592
Second-order	K_2 (min^{-1})	q_e (mg/g)	R^2
RRC	0.0736	25.189	0.999
SRC	0.0379	4.593	0.991

According to the presented results, the Lagergren PFO kinetic model data do not obey straight lines according to linear fitting factor R^2 (0.342 on RRC and 0.592 on SRC) indicating that the fitting of this model was not adequate. In contrast, the PSO kinetic model data were found to be the best fit as indicated from the high values of R^2 correlation coefficient for MB adsorption (0.999 on RRC and 0.991 on SRC). Evidently, the Ho and McKay PSO kinetic model can be applied to predict the amount of dye uptake at different contact time intervals and at equilibrium. From Table 2 it is observed that for the studied condition, the PSO expression accurately predicts the adsorption kinetics rather than the PFO model. Furthermore, the adsorption mechanism is driven by chemical sorption, which is a velocity controlling process. The same findings are reported in the literature [36,43,44].

3.2.3. pH effect

The batch pH is an important factor that influences materials surface charge. In order to understand the character of studied samples at different pH, pH_{PZC} point was determined by plotting the evolution of ΔpH vs. initial pH as shown in Fig. 9.

As a result, RRC and SRC present similar pH_{PZC} points around pH 8. Both samples show a negative charge in the range of pH from 2 to 8 and positive charge beyond pH 8. It seems that based on the pH_{PZC} that is equivalent to the zeta potential null, the adsorption of cationic dyes on RRC and SRC is favorable and is recommended under pH < 8.

To understand the effect of ionic species on solid surface potential, it is important to distinguish between irrelevant ions, potential-determining ions, and surface-active electrolytes. Neutral ions are ionic species that cause a change in zeta potential closer to zero (ΔpH = 0). The only type of interaction between these ions and the surface is electrostatic attraction, which disappears when the surface is neutralized, so that no further extraneous ions can be adsorbed [45].

Furthermore, potential-determining ions can change the zeta potential of the electric double layer because they interact with the particle surface, not just through electrostatic interactions [46].

In this case, pH effect was studied in the range of 2–10 with initial MB concentration of 50 ppm at room temperature (25°C ± 1°C) during 20 and 30 min respectively for RRC and SRC. The adsorption of MB at different pH is illustrated in Fig. 10. From the obtained profile, adsorption of MB onto RRC was favorable and stable at all pH mediums. This can be due to the high effective charges on the clay surface [47].

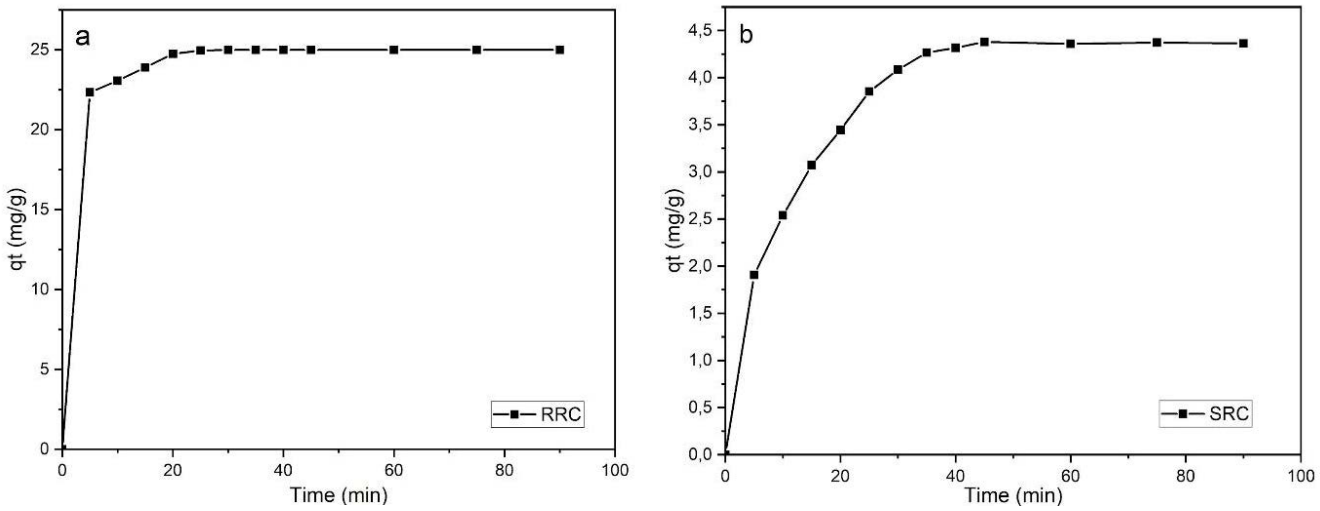

Fig. 7. Effect of contact time on raw red clay (a) and sintered red clay (b) adsorption capacity for MB removal.

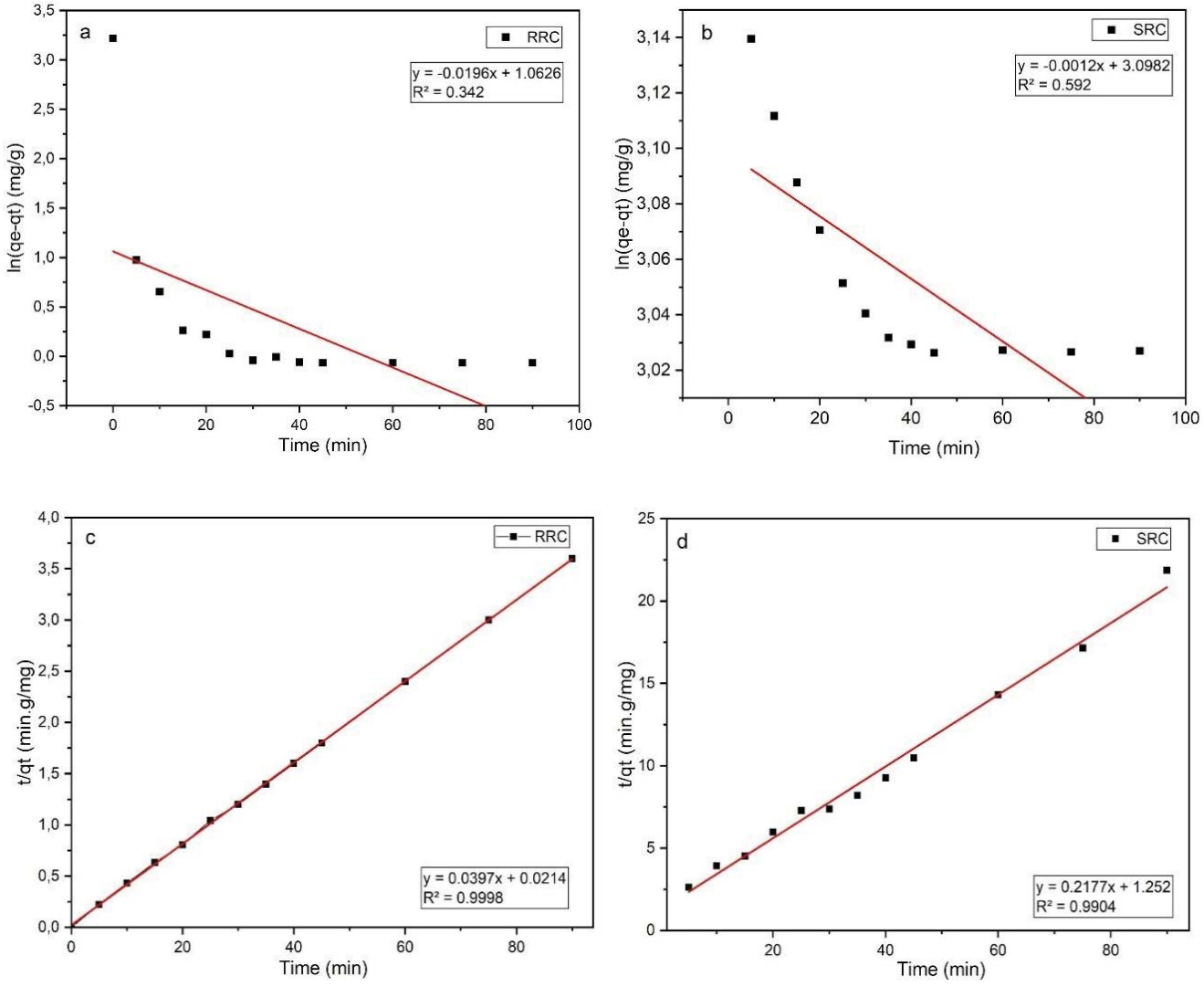

Fig. 8. Adsorption kinetic models: (a and b) pseudo-first-order and (c and d) pseudo-second-order.

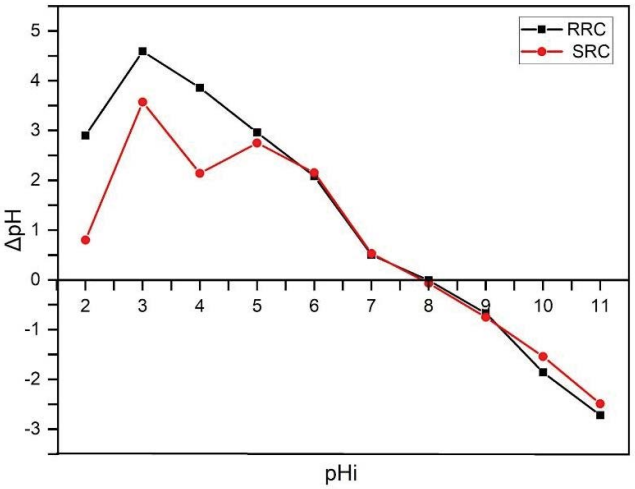

Fig. 9. pH_{PZC} of raw red clay and sintered red clay.

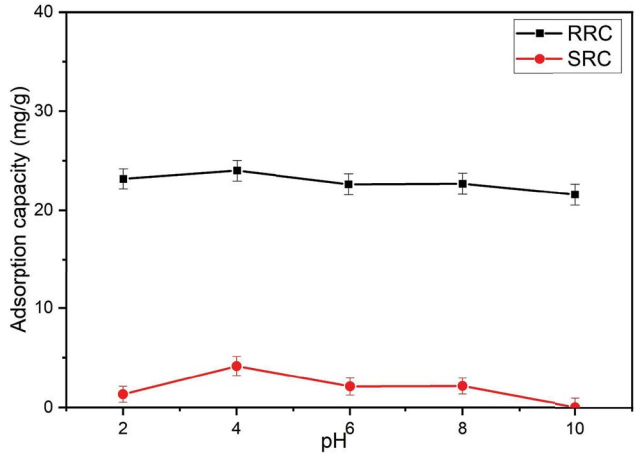

Fig. 10. pH effect on adsorption capacity of raw red clay and sintered red clay.

Therefore, the adsorption of MB into SRC was unfavorable at pH > 8. SRC shows a minimal adsorption capacity in acidic and basic media and has a tendency to be favored at initial pH slightly acidic (between 4 and 6). The maximum adsorption capacity was obtained at the initial solution of pH 4 to be 24 and 4 mg/g respectively for RRC and SRC. The observed decrease in terms of dye adsorption in basic and acidic mediums can be related to the high interactions between protons in acidic medium and hydroxyls in the basic medium. Soft increase in terms of MB adsorption is due to the increased electrostatic interactions between cationic dye molecules and the sample surface. This is due to the deprotonation of active sites of the surface, which means that a decrease in the surface charge density of the adsorbent occurs with increasing pH [28].

However, the electrostatic adsorption process in basic medium cannot explain the slight decrease in MB removal at pH 8–10. This diminution could be another mode of adsorption such as chelation ion exchange that results in MB removal decrease at higher pH [48]. Finally, the pH between 4 and 8 was preferred to study the effect of other adsorption parameters.

3.2.4. Concentration effect

The influence of the initial MB dye concentration on adsorption equilibrium was performed in the range of 20–70 ppm at optimum time of each sample, while the other optimal conditions such as adsorbent dose (0.1 g and 0.2 respectively for RRC and SRC), solution pH (5.8) and temperature (298 K) were held constant. Fig. 11 shows the equilibrium adsorption capacity as function of MB initial concentration for both adsorbents.

Fig. 11 reveals that RRC presents a higher adsorption capacity q_t (mg/g) than SRC under the same conditions. In the case of SRC, MB removal began from 80% at lowest concentration of 20 ppm, which can be explained by the saturation of superficial and structural sites of SRC. This incapability to remove the totality of MB molecules lead to a decrease in capacity as function of concentration. This result is in accordance with previous results. On other hand, RRC presents a removal rate of 100% in the range from 0 to 40 ppm before it decreases, this can be explained by the insaturation of clay surface and structural sites [49]. From the obtained results, it can be concluded that RRC presents a maximum adsorption capacity for MB elimination at the concentration of 40 ppm, meanwhile for SRC sample, the maximum of adsorption capacity is given at less than 20 ppm. Additionally, the obtained results are in concordance with the BET surface area analysis, which reveal that RRC surface is twice that of SRC.

3.2.5. Adsorption isotherm

The adsorption isotherm studies provide useful information into adsorption mechanisms as well as surface properties and affinity of the adsorbents. The obtained experimental data of MB adsorption onto RRC and SRC at equilibrium were analyzed by Langmuir and Freundlich isotherm models, the most used models for the expression of adsorption modelization [9,44]. As mentioned in Eq. (5), the Langmuir isotherm is based on the hypothesis of monolayer adsorption in which the process takes place at specific temperatures. Additionally, the adsorbent surface is considered homogeneous and each dye molecule occupies a unique site. The linear form of the Langmuir isotherm model can be expressed as follow:

$$\frac{1}{Q_e} = \frac{1}{Q_m} + \left(\frac{1}{Q_m K_L}\right)\frac{1}{C_e} \tag{5}$$

where Q_e, Q_m and K_L are the adsorption capacity corresponding to the MB equilibrium concentration C_e, the maximum adsorption amount of metal ions (mg/g) and the Langmuir adsorption constant (L/mg) respectively.

On other hand, Freundlich isotherm is an empirical model in which the adsorption process is conducted on a multilayer adsorption mechanism and heterogeneous surface. Moreover, the adsorption capacity is directly related to the equilibrium concentration. The linear form of the Freundlich isotherm model can be expressed as given in Eq. (6):

$$\log Q_e = \log K_f + \frac{1}{n}\log C_e \quad (6)$$

where K_f and n are the constants of the adsorption model and empirical constant that indicates adsorption intensity respectively. The experimental data of Langmuir and Freundlich isotherms for RRC and SRC samples are given in Fig. 12a–d, respectively. The constant values corresponding to each model are summarized in Table 3.

For Langmuir isotherm, the fitting plots of $1/Q_e$ vs. $1/C_e$ for RRC and SRC leads to a linear curve with $1/q_m K_L$ as a slope and $1/q_m$ as intercept (Fig. 12a and b). The value of q_m indicates the maximum adsorption capacity of both samples. The adaptability of the model is determined from the value of correlation coefficient (R^2). On the other hand, Freundlich isotherm fitting plots of $\ln(Q_e)$ vs. $\ln(C_e)$ for RRC and SRC are given in (Fig. 12c and d). The value of $1/n$ gives an indication of the validity of the adsorption of MB onto the sample surface. A value of $1/n$ between 0 and 1 indicates favorable adsorption [28–30,48]. The numerical values of q_m, K_L, K_f and $1/n$ calculated respectively for RRC and SRC are reported in Table 3.

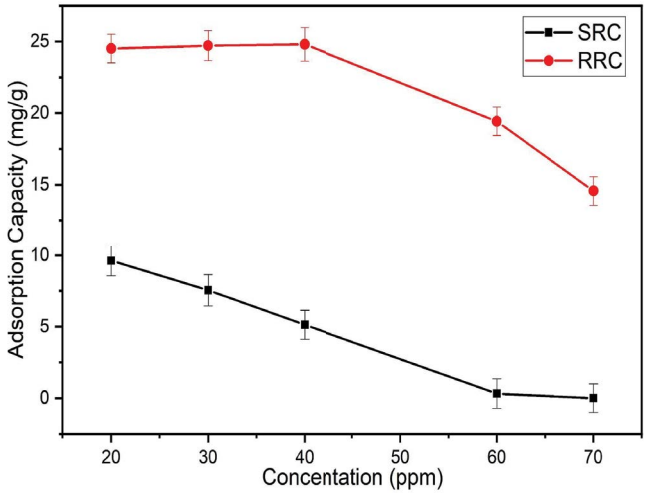

Fig. 11. Effect of concentration of sintered red clay and raw red clay.

Table 3
Isotherm model parameters for MB adsorption onto RRC and SRC

Langmuir				
Adsorbent	Intercept	q_m	K_L	R^2
RRC	0.074	135.135	0.009	0.969
SRC	0.316	3.129	0.189	0.978
Freundlich				
Adsorbent	Intercept	$1/n$	K_f	R^2
RRC	2.870	0.093	17.646	0.174
SRC	0.082	0.186	1.390	0.935

The Table 3 shows the values of the Langmuir and Freundlich parameters. From the fitting plots and based on R^2 values, it appears that the Langmuir model expresses the adsorption better than Freundlich. As a result, it can be concluded that the adsorption on RRC and SRC is favorable. Moreover, the adsorption of MB on RRC is more highly described by Langmuir model than Freundlich with a maximum capacity of 135.135 mg/g. In the case of SRC, both models are applicable for the description of MB adsorption. It can be concluded that MB molecules present a good affinity to the RRC surface. In contrast, SRC presents a low affinity to MB according to both models. The same results have been demonstrated for muscovite clay by several authors [28–30].

3.2.6. Adsorption thermodynamic

The influence of temperature was studied in the range of 20°C–60°C. The tests were performed on 50 mL mixtures of dye solution at concentration of 50 ppm, with 0.1 and 0.2 g of weight for RRC and SRC respectively at initial pH of 5.8. The mixtures were kept under stirring rate of 250 rpm for an optimal time of 20 and 30 min respectively for RRC and SRC.

Fig. 13 shows MB removal using RRC and SRC as a function of temperature. The influence of batch temperature directly affects the adsorption process. From the Fig. 13, it can be shown that RRC presents a slight decrease in terms of adsorption rate when temperature increases from 20°C to 60°C. Moreover, SRC presents a significant decrease of 50% in adsorption capacity. The adsorption thermodynamic for two samples obtained at different temperatures is used to detect and describe the adsorption mechanism as presented in Fig. 13.

Using the Van't Hoff law equation (Eq. 7a) [50], the integral of adsorption heat was calculated from K_d variation. This variation is calculated from the slope and intersection of the plot of $\ln K_d$ vs. $1/T$ using Eq. (7b).

$$G° = \Delta H° - T\Delta S° \quad (7a)$$

$$\ln K_d = \frac{\Delta S°}{R} - \frac{\Delta H°}{RT} \quad (7b)$$

where K_d, T, $\Delta S°$, $\Delta H°$ and R are distribution coefficient (L/g), absolute temperature (K), entropy change (J/mol K), standard enthalpy (J/mol) and ideal gas constant (8.314 J/mol K) respectively. The plots of $\ln K_d$ as a function of $1/T$ is illustrated in the Fig. 14:

Enthalpy and entropy values were obtained from the linear plot of the variation of $\ln(K_d)$ as function of $1/T$ (Fig. 14); $\Delta H°/R$ and $\Delta S°/R$ are the slope and intercept, respectively. From the Fig. 14, the evolution is linear with an R^2 close to 1 for both samples. The values of the thermodynamic adsorption parameters of MB dye on RRC and SRC are grouped in Table 4.

Table 4 presents experimental values of standard free energy, standard entropy and standard enthalpy. These parameters are extrapolated from the plot of $\ln(K_d)$ vs. $(1/T)$ given by the linear regression of experimental data.

The $\Delta H°$ values for RRC and SRC are equal to –16,802.59 and –28,383.99 kJ/mol, respectively. The negative values

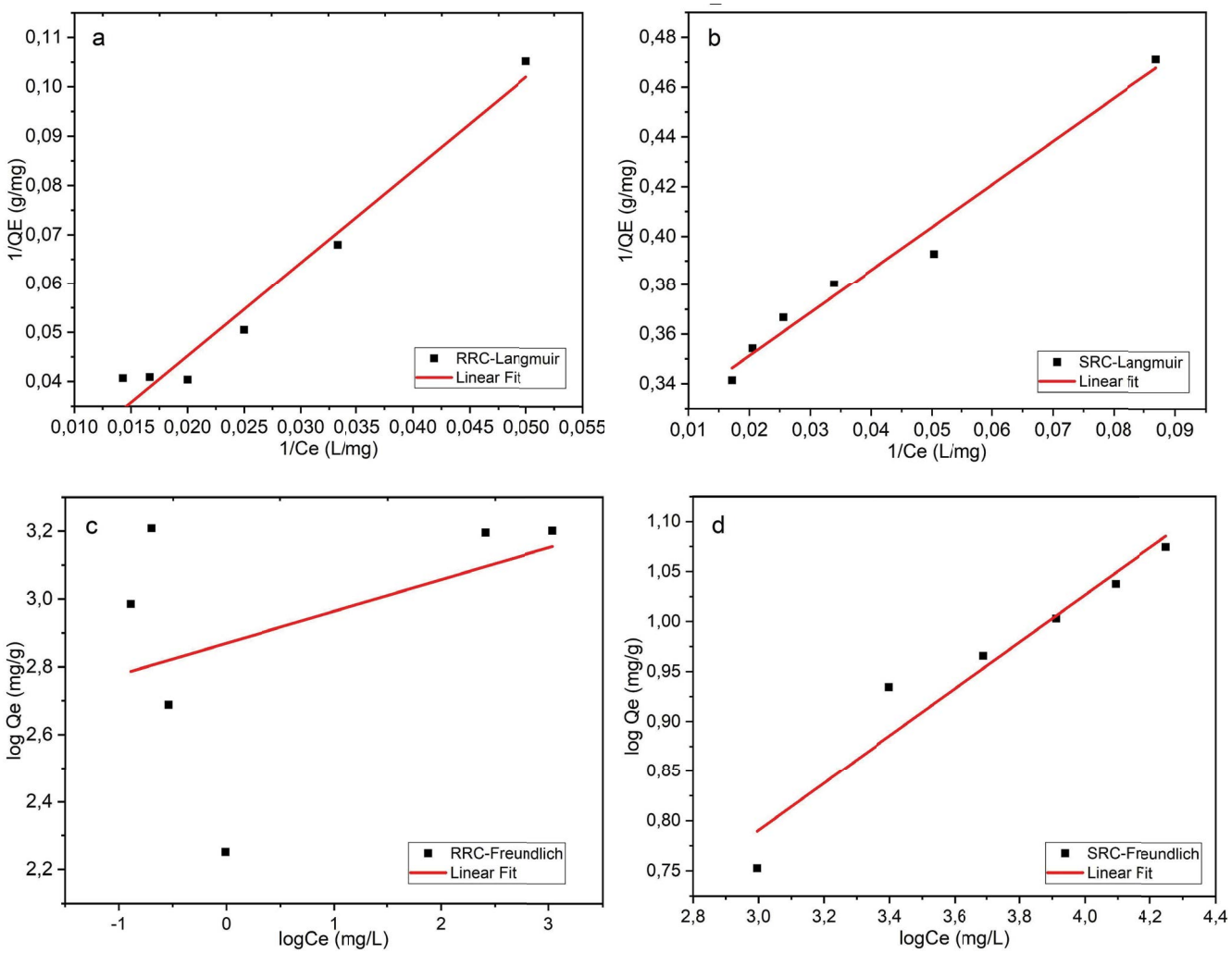

Fig. 12. Freundlich and Langmuir isotherms for MB adsorption on raw red clay and sintered red clay.

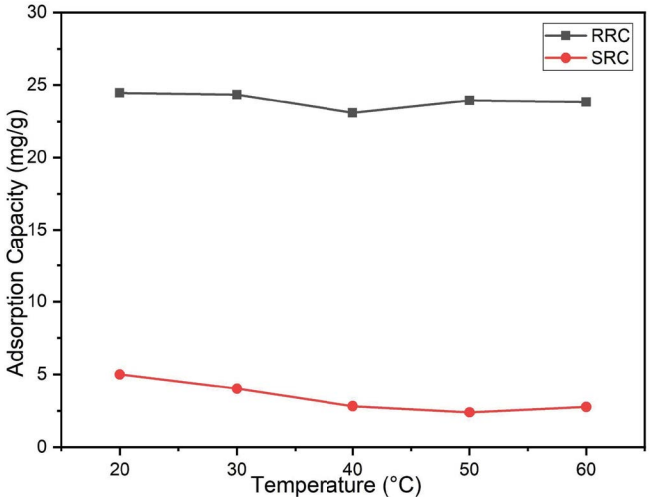

Fig. 13. Effect of temperature on MB adsorption using raw red clay and sintered red clay.

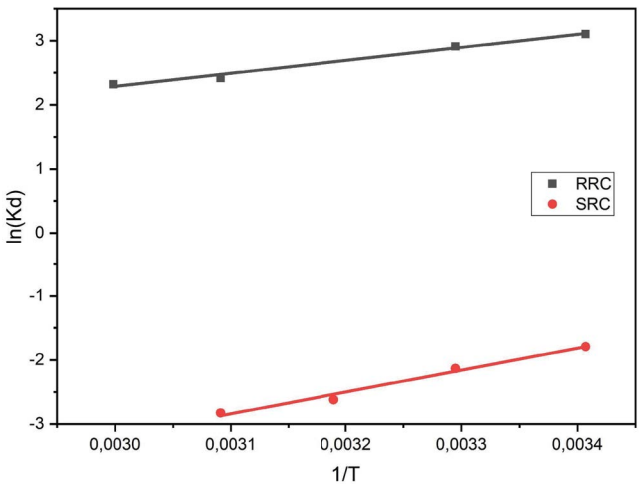

Fig. 14. Adsorption thermodynamic of sintered red clay and raw red clay.

Table 4
Adsorption thermodynamic parameters of MB using RRC and SRC

Sample	RRC	SRC
$\Delta G°$ (kJ/mg)	–7.596	4.370
$\Delta S°/R$	–3.773	–13.423
$\Delta H°/R$	–2,021	–3,414
$\Delta S°$ (J/mol·K)	–31.370	–111.600
$\Delta H°$ (kJ/mol)	–16,802.590	–28,383.990
R^2	0.988	0.983

of this parameter indicate that the reaction is exothermic. We can conclude that the more temperature increases, the more adsorption decreases. The distribution order of dye molecules on the adsorbent increases dependently with the solution. The values of $\Delta S°$ are found to be –31.36 and –111.59 J/mol·K for the adsorption of MB on RRC and SRC respectively. The negative values of $\Delta S°$ suggest a decrease in the randomness at the solid/solution interface during the adsorption of MB dye molecules onto SRC and RRC [51].

The plot of free energy $\Delta G°$ vs. temperature as shown in Fig. 15 describes the adsorption of MB and discloses that it is thermodynamically feasible on the RRC sample and judged by the negative value of $\Delta G°$. The process is naturally spontaneous in the range of 20°C–60°C. On other hand, regarding the positive $\Delta G°$ value for the SRC adsorbent, it indicates that the process is feasible but not spontaneous for MB cations. Therefore, the $\Delta G°$ increased by increasing the temperature which indicates limitation of the SRC system for MB adsorption.

4. Limitations and perspectives

Based on the obtained results, the application of red clay as an adsorbent in industrial scale should be limited by several parameters such as surface affinity. Red clay can be used to clarify liquid effluents of positively charged pollutants as the case of this study (methylene blue dye). But on the other hand, the studied clay cannot be a good adsorbent for the removal of negatively charged pollutants. For this reason, this clay could not be a good candidate for various industrial effluents. Additionally, the red clay is still very useful for specific uses. According to the obtained results, the thermal treatment at high temperature makes impossible the regeneration of this clay surface due to the inactivation of the active sites on the surface by oxidation or partial melting. On the other hand, the application of red clay in other processes such as the treatment of ceramics can be a good solution for several problems. For example, the elaboration of a low-cost ceramic membranes from red clay sintered at high temperature, allows bringing a good solution to the phenomenon of fouling.

5. Conclusion

Red clay can be used as a good adsorbent for methylene blue removal from wastewater. Fourier transforms infrared analysis, specific area, X-ray diffraction, and thermal analysis

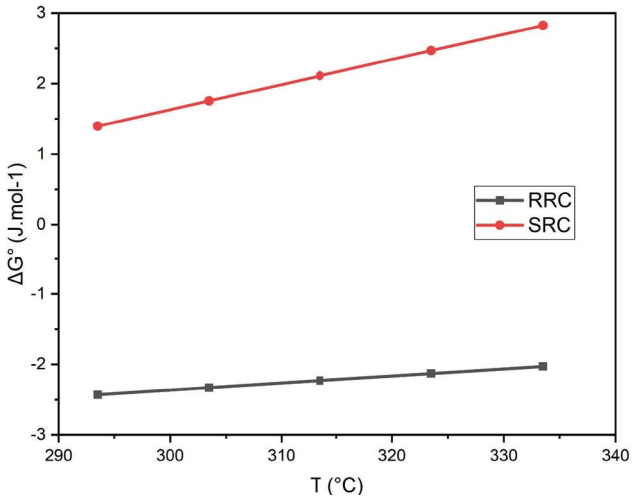

Fig. 15. The evolution of free energies vs. temperature.

(TGA) characterization techniques are applied to identify studied clay samples. Kinetic and isotherms adsorption models were used to study the adsorption potential of the clay for the removal of methylene blue in aqueous solution and demonstrated a maximum adsorption capacity of about 25 and 5 mg/g respectively for RRC and SRC. The kinetic models indicated that the adsorption process of methylene blue on clay for both samples obeyed the PSO model (R^2 correlation coefficient egal 0.999 on RRC and 0.991 on SRC). The Langmuir isotherm model was found to be more appropriate for predicting the adsorption of methylene blue onto studied samples with a maximum capacity of 135.135 mg/g.

All these results confirm the potential of this clay to be used in the field of organic pollutants remediation. On the other hand, the thermal treatment of this clay at 950°C reduces the BET surface area and makes red clay inactive for the removal of MB which is confirmed by the obtained lowest rates. This result is very significant in investigating the behavior of sintered red clay SRC in other applications such as ceramic membrane manufacturing, especially to treat the problem of membrane fouling.

References

[1] R. Croce, F. Cinà, A. Lombardo, G. Crispeyn, C.I. Cappelli, M. Vian, S. Maiorana, E. Benfenati, D. Baderna, Aquatic toxicity of several textile dye formulations: acute and chronic assays with *Daphnia magna* and *Raphidocelis subcapitata*, Ecotoxicol. Environ. Saf., 144 (2017) 79–87.
[2] M. Ali, T.R. Sreekrishnan, Aquatic toxicity from pulp and paper mill effluents: a review, Adv. Environ. Res., 5 (2001) 175–196.
[3] A. Karim, B. Achiou, A. Bouazizi, A. Aaddane, M. Ouammou, M. Bouziane, J. Bennazha, S. Alami Younssi, Development of reduced graphene oxide membrane on flat Moroccan ceramic pozzolan support. Application for soluble dyes removal, J. Environ. Chem. Eng., 6 (2018) 1475–1485.
[4] N.M. Mahmoodi, M. Taghizadeh, A. Taghizadeh, Mesoporous activated carbons of low-cost agricultural bio-wastes with high adsorption capacity: preparation and artificial neural network modeling of dye removal from single and multicomponent (binary and ternary) systems, molliq, 269 (2018) 217–228.
[5] B. Nicolaisen, Developments in membrane technology for water treatment, Desalination, 153 (2003) 355–360.

[6] A. Srivastava, V.K. Parida, A. Majumder, B. Gupta, A.K. Gupta, Treatment of saline wastewater using physicochemical, biological, and hybrid processes: insights into inhibition mechanisms, treatment efficiencies and performance enhancement, J. Environ. Chem. Eng., 9 (2021) 105775, doi: 10.1016/j.jece.2021.105775.
[7] S. Sadri Moghaddam, M.R. Alavi Moghaddam, M. Arami, Coagulation/flocculation process for dye removal using sludge from water treatment plant: optimization through response surface methodology, J. Hazard. Mater., 175 (2010) 651–657.
[8] D.M. Ruthven, Fundamentals of Adsorption Equilibrium and Kinetics in Microporous Solids. Adsorption and Diffusion, Springer, Berlin, Heidelberg, 2006, pp. 1–43.
[9] M.T. Yagub, T.K. Sen, S. Afroze, H.M. Ang, Dye and its removal from aqueous solution by adsorption: a review, Adv. Colloid Interface Sci., 209 (2014) 172–184.
[10] A. Singh, D.P. Dutta, J. Ramkumar, K. Bhattacharya, A.K. Tyagi, M.H. Fulekar, Serendipitous discovery of super adsorbent properties of sonochemically synthesized nano $BaWO_4$, RSC Adv., 3 (2013) 22580–22590.
[11] G.L. Dotto, G. McKay, Current scenario and challenges in adsorption for water treatment, J. Environ. Chem. Eng., 8 (2020) 103988, doi: 10.1016/j.jece.2020.103988.
[12] W.H. Lee, P.J. Reucroft. Vapor adsorption on coal- and wood-based chemically activated carbons(II) adsorption of organic vapors, Carbon, 37 (1999) 15–20.
[13] R. Kant, Adsorption of dye eosin from an aqueous solution on two different samples of activated carbon by static batch method, J. Water Res. Prot., 4 (2012) 93–98.
[14] T.N.V. de Souza, S.M.L. de Carvalho, M.G.A. Vieira, M.G.C. da Silva, D. do S.B. Brasil, Adsorption of basic dyes onto activated carbon: experimental and theoretical investigation of chemical reactivity of basic dyes using DFT-based descriptors, Appl. Surf. Sci., 448 (2018) 662–670.
[15] M. Arami, N.Y. Limaee, N.M. Mahmoodi, N.S. Tabrizi, Removal of dyes from colored textile wastewater by orange peel adsorbent: equilibrium and kinetic studies, J. Colloid Interface Sci., 288 (2005) 371–376.
[16] X. Zhou, L. Shi, T.B. Moghaddam, M. Chen, S. Wu, X. Yuan, Adsorption mechanism of polycyclic aromatic hydrocarbons using wood waste-derived biochar, J. Hazard. Mater., 425 (2022) 128003, doi: 10.1016/j.jhazmat.2021.128003.
[17] M. Daoud, O. Benturki, Z. Kecira, P. Girods, A. Donnot, Removal of reactive dye (BEZAKTIV Red S-MAX) from aqueous solution by adsorption onto activated carbons prepared from date palm rachis and jujube stones, J. Mol. Liq., 243 (2017) 799–809.
[18] N. El Ouahedy, M. Zbair, S. Ojala, R. Brahmi, L. Pirault-Roy, Porous carbon materials derived from olive kernels: application in adsorption of organic pollutants, Environ. Sci. Pollut. Res., 27 (2020) 29967–29982.
[19] D.P. Dutta, S. Nath, Low-cost synthesis of SiO_2/C nanocomposite from corn cobs and its adsorption of uranium(VI), chromium(VI) and cationic dyes from wastewater, J. Mol. Liq., 269 (2018) 140–151.
[20] N. Fayoud, S. Tahiri, S. Alami Younssi, A. Albizane, D. Gallart-Mateu, M.L. Cervera, M. de la Guardia, Kinetic, isotherm and thermodynamic studies of the adsorption of methylene blue dye onto agro-based cellulosic materials, Desal. Water Treat., 57 (2016) 16611–16625.
[21] Y. Dehmani, O. El Khalki, H. Mezougane, S. Abouarnadasse, Comparative study on adsorption of cationic dyes and phenol by natural clays, Chem. Data Collect., 33 (2021) 100674, doi: 10.1016/j.cdc.2021.100674.
[22] M. Ahrouch, J.M. Gatica, K. Draoui, H. Vidal, Adding value to natural clays as low-cost adsorbents of methylene blue in polluted water through honeycomb monoliths manufacture, SN Appl. Sci., 1 (2019) 1595, doi: 10.1007/s42452-019-1636-4.
[23] H. Bensalah, S.A. Younssi, M. Ouammou, A. Gurlo, M.F. Bekheet, Azo dye adsorption on an industrial waste-transformed hydroxyapatite adsorbent: kinetics, isotherms, mechanism and regeneration studies, J. Environ. Chem. Eng., 8 (2020) 103807, doi: 10.1016/j.jece.2020.103807.
[24] G. Derouich, S.A. Younssi, J. Bennazha, B. Achiou, M. Ouammou, I.E.E. El-Hassani, A. Albizane, Adsorption study of cationic and anionic dyes onto Moroccan natural pozzolan. Application for removal of textile dyes from aqueous solutions, Desal. Water Treat., 145 (2019) 348–360.
[25] M. Doğan, M. Alkan, A. Türkyilmaz, Y. Özdemir, Kinetics and mechanism of removal of methylene blue by adsorption onto perlite, J. Hazard. Mater., 109 (2004) 141–148.
[26] A.H. Jawad, A.S. Abdulhameed, Mesoporous Iraqi red kaolin clay as an efficient adsorbent for methylene blue dye: adsorption kinetic, isotherm and mechanism study, Surf. Interfaces, 18 (2020) 100422, doi: 10.1016/j.surfin.2019.100422.
[27] M.C. Avila, I.D. Lick, N.A. Comelli, M.L. Ruiz, Adsorption of an anionic dye from aqueous solution on a treated clay, Groundwater Sustainable Dev., 15 (2021) 100688, doi: 10.1016/j.gsd.2021.100688.
[28] O. Amrhar, A. Berisha, L. El Gana, H. Nassali, M.S. Elyoubi, Removal of methylene blue dye by adsorption onto natural Muscovite clay: experimental, theoretical and computational investigation, J. Environ. Anal. Chem., (2021) 1–26, doi: 10.1080/03067319.2021.1897119.
[29] M.A. Salam, M.R. Abukhadra, M. Mostafa, Effective decontamination of As(V), Hg(II), and U(VI) toxic ions from water using novel muscovite/zeolite aluminosilicate composite: adsorption behavior and mechanism, Environ. Sci. Pollut. Res., 27 (2020) 13247–13260.
[30] M.A. Barakat, R. Kumar, E.C. Lima, M.K. Seliem, Facile synthesis of muscovite–supported Fe_3O_4 nanoparticles as an adsorbent and heterogeneous catalyst for effective removal of methyl orange: characterisation, modelling, and mechanism, J. Taiwan Inst. Chem. Eng., 119 (2021) 146–157.
[31] M.Á. López Zavala, H. Romero-Santana, B.E. Monárrez-Cordero, Removal of Cr(VI) from water by adsorption using low cost clay-perlite-iron membranes, J. Water Process Eng., 38 (2020) 101672, doi: 10.1016/j.jwpe.2020.101672.
[32] Y. Rakhila, A. Ezzahi, A. Elmchaouri, A. Mestari, Synthesis and characterization of a red clay based new composite ceramic material, Adv. Mater. Phys. Chem., 8 (2018) 295–310.
[33] Y. Rakhila, A. Elmchaouri, A. Mestari, S. Korili, M. Abouri, A. Gil, Adsorption recovery of Ag(I) and Au(III) from an electronics industry wastewater on a clay mineral composite, Int. J. Miner. Metall. Mater., 26 (2019) 673–680.
[34] R. Ozao, M. Ochiai, A. Yamazaki, R. Otsuka, Thermal analysis of ground dolomites, Thermochim. Acta, 183 (1991) 183–198.
[35] B. Achiou, H.E. Omari, J. Bennazha, A. Albizane, L. Daoudi, L. Saadi, M. Ouammou, S.A. Younssi, A.E. Maadi, M. Chehbouni, Physicochemical and mineralogical characterizations of clays from Fez region (basin of Saiss, Morocco) in the perspective of industrial use, J. Mater. Environ. Sci., 7 (2016) 1474–1484.
[36] M.M. Rahman, S.H. Rimu, S. Biswas, T.U. Rashid, A.H. Chisty, M.A. Rahman, S. Murad, P. Haque, Preparation of poly(acrylic acid) exfoliated clay composite by *in-situ* polymerisation for decolouration of methylene blue from wastewater, Int. J. Environ. Anal. Chem., (2020), doi: 10.1080/03067319.2020.1813732.
[37] B.K. Shahraki, B. Mehrabi, K. Gholizadeh, M. Mohammadinasab, Thermal behavior of calcite as an expansive agent, J. Min. Metall. Sect. B., 47 (2011) 89–97.
[38] J. Bertaux, F. Froehlich, P. Ildefonse, Multicomponent analysis of FTIR spectra; quantification of amorphous and crystallized mineral phases in synthetic and natural sediments, J. Sediment. Res., 68 (1998) 440–447.
[39] H. Ouaddari, A. Karim, B. Achiou, S. Saja, A. Aaddane, J. Bennazha, I.E.A. El Hassani, M. Ouammou, A. Albizane, New low-cost ultrafiltration membrane made from purified natural clays for direct Red 80 dye removal, J. Environ. Chem. Eng., 7 (2019) 103268, doi: 10.1016/j.jece.2019.103268.
[40] H. Elomari, B. Achiou, M. Ouammou, A. Albizane, J. Bennazha, S. Alami Younssi, I. Elamrani, Elaboration and characterization of flat membrane supports from Moroccan clays. Application for the treatment of wastewater, Desal. Water Treat., 57 (2016) 20298–20306.
[41] B. Achiou, H. Elomari, A. Bouazizi, A. Karim, M. Ouammou, A. Albizane, J. Bennazha, S.A. Younssi, I.E. El Amrani,

Manufacturing of tubular ceramic microfiltration membrane based on natural pozzolan for pretreatment of seawater desalination, Desalination, 419 (2017) 181–187.
[42] Y. Dehmani, L. Sellaoui, Y. Alghamdi, J. Lainé, M. Badawi, A. Amhoud, A. Bonilla-Petriciolet, T. Lamhasni, S. Abouarnadasse, Kinetic, thermodynamic and mechanism study of the adsorption of phenol on Moroccan clay, J. Mol. Liq., 312 (2020) 113383, doi: 10.1016/j.molliq.2020.113383.
[43] R.A. Shawabkeh, M.F. Tutunji, Experimental study and modeling of basic dye sorption by diatomaceous clay, Appl. Clay Sci., 24 (2003) 111–120.
[44] Ravi, L.M. Pandey, Enhanced adsorption capacity of designed bentonite and alginate beads for the effective removal of methylene blue, Appl. Clay Sci., 169 (2019) 102–111.
[45] M. Markiewicz, W. Mrozik, K. Rezwan, J. Thöming, J. Hupka, C. Jungnickel, Changes in zeta potential of imidazolium ionic liquids modified minerals – implications for determining mechanism of adsorption, Chemosphere, 90 (2013) 706–712.
[46] D.W. Fuerstenau, Pradip, Zeta potentials in the flotation of oxide and silicate minerals, Adv. Colloid Interface Sci., 114–115 (2005) 9–26.
[47] E.N. El Qada, S.J. Allen, G.M. Walker, Adsorption of basic dyes from aqueous solution onto activated carbons, J. Chem. Eng., 135 (2008) 174–184.
[48] S. Tang, Z. Wang, D. Yuan, C. Zhang, Y. Rao, Z. Wang, K. Yin, Ferrous ion-tartaric acid chelation promoted calcium peroxide Fenton-like reactions for simulated organic wastewater treatment, J. Cleaner Prod., 268 (2020) 122253, doi: 10.1016/j.jclepro.2020.122253.
[49] A.R. Tehrani-Bagha, H. Nikkar, N.M. Mahmoodi, M. Markazi, F.M. Menger, The sorption of cationic dyes onto kaolin: kinetic, isotherm and thermodynamic studies, Desalination, 266 (2011) 274–280.
[50] M.E. González-López, C.M. Laureano-Anzaldo, A.A. Pérez-Fonseca, M. Arellano, J.R. Robledo-Ortíz, A critical overview of adsorption models linearization: methodological and statistical inconsistencies, Sep. Purif. Rev., 51 (2022) 358–372.
[51] T. Shen, L. Wang, Q. Zhao, S. Guo, M. Gao, Single and simultaneous adsorption of basic dyes by novel organo-vermiculite: a combined experimental and theoretical study, Colloids Surf., A, 601 (2020) 125059, doi: 10.1016/j.colsurfa.2020.125059.

Appendix

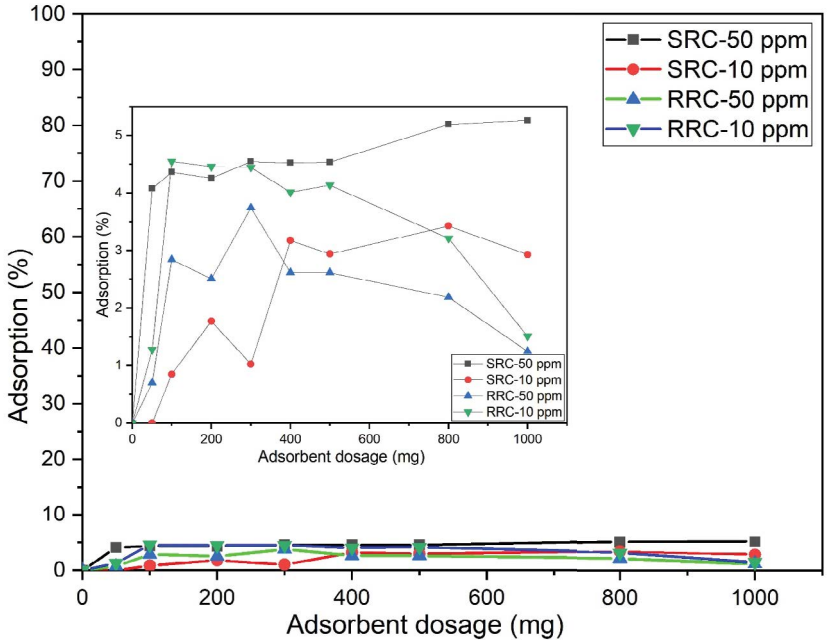

Appendix A: Dose effect of raw red clay and sintered red clay for methyl orange removal at concentration of 10 and 50 ppm.